Journal of Applied Polymer Science

Reinforcement of ethylene-acrylic elastomer with a dispersion of grafted PA6 droplets

S. R. Oriani
DuPont, 200 Powder Mill Road, Wilmington, Delaware, 19803
Correspondence to: S. R. Oriani (E-mail: steve.r.oriani@dupont.com)

ABSTRACT: Cured elastomers are commonly dispersed in thermoplastics, but the reverse morphology has received little attention. The present work examines dispersions of 0.5–2 μm PA6 droplets in ethylene-acrylic elastomer (AEM), created by melt blending. After cooling, the blends are compounded with amine curative and crosslinked. Uncrosslinked blends exhibit high bound rubber levels compared to N990 carbon black filled AEM, but similar viscosity at equal filler volume fraction. Crosslinking the blends produces strong, heat resistant vulcanizates with minimal Payne effect and good compression set resistance. These properties result from extensive AEM-PA6 grafting, absence of filler-filler contacts, and beneficial modification of the oxidation profile under diffusion limited conditions. The data show rubber-filler grafting strongly influences filler reinforcing ability, but does not directly influence the Payne effect. Relative to unfilled AEM, silica and carbon black fillers accelerate oxidative degradation in proportion to their reinforcing ability, whereas PA6 has a stabilizing effect. © 2016 Wiley Periodicals, Inc. J. Appl. Polym. Sci. **2016**, *133*, 43995.

KEYWORDS: blends; elastomers; rubber

Received 11 September 2015; accepted 25 May 2016
DOI: 10.1002/app.43995

INTRODUCTION

Virtually all thermoset rubber compounds contain particulate filler. Carbon black and silica are among the most commonly used to increase strength and modulus of a cured rubber article, while lower surface area fillers such as calcium carbonate or clay function as extenders to decrease compound cost. An enormous literature has evolved over the past half-century with the goal of describing how carbon black and various inorganic fillers affect rubber properties, both before and after curing.[1–6] Complications arise because of filler structure and filler-filler interactions,[1–7] dispersion of the filler,[8–10] polymer-filler interactions including bound and occluded rubber,[1–7,9–14] cure inhibition or acceleration at the filler surface,[3,6] filler particle radius,[14,15] and filler anisotropy.[16]

On the other hand, relatively little attention has been given to reinforcement of elastomers with a dispersion of non-elastomeric polymer droplets. Perhaps the first published reference describes emulsion polymerization of butadiene, using a seed polymer of polyacrylonitrile.[17] Vulcanization yielded strong, oxidation resistant elastomers without the need for carbon black. Other workers have used emulsion polymerized styrene, styrene-butadiene, 2,6-dicholorstyrene, acenaphthylene, methylmethacrylate, or tetrafluoroethylene to produce polymer spheres varying from about 0.3 to 1.7 μm diameter, subsequently dispersed within a continuous phase of SBR or polysulfide elastomer.[18–20] The relatively high modulus polymer particles increased tensile strength and elongation at break of the vulcanizates compared to unfilled controls. The polymeric fillers did not, however, yield property advantages compared to conventional fillers.[20]

Industrially, elastomer reinforcement by a dispersion of thermoplastic is uncommon, possibly because the approach tends to cause more problems than it solves. For example, polystyrene may be blended into styrene-butadiene rubber compounds to improve processability, at the expense of severe property loss at elevated temperatures. Polyvinylchloride may be blended with nitrile rubber to improve weatherability, while sacrificing elasticity.[21] A practical difficulty in polymeric reinforcement of elastomers is that few thermoplastics are commercially available in sufficiently small particle size – 1 μm diameter is cited as the maximum for significant reinforcement of elastomers.[2] Small particle polytetrafluoroethylene (PTFE) powders are available and find use, particularly in fluoroelastomers, which can absorb their high cost in specialized applications. PTFE powders can increase tear strength, abrasion resistance, and lubricity of various elastomers, but are not considered a substitute for conventional fillers like carbon black or silica.[22,23]

Rubber engineers have also created dispersions of thermoplastics in thermoset elastomers by melt blending the uncured elastomer with thermoplastic, cooling to solidify the plastic, followed by

Table I. Properties of Carbon Black and Silica Fillers

	Primary particle size (nm)	Surface area (m^2/g)[a]	DBP oil absorption (mL/100 g)[b]
N990 (MT) carbon black	200-500	8-10	43
N330 (HAF) carbon black	26-30	76	102
Silica (precipitated)	14	170	200

[a] ASTM D3037.
[b] ASTM D2414.

conventional rubber compounding to add curative and other ingredients. The technique has been applied to fluoroelastomer-fluoroplastic blends as well as ethylene-propylene diene monomer rubber (EPDM) containing polyamide fibers created *in situ*.[24–27] The most relevant work, however, involves cured EPDM and hydrogenated nitrile rubber (HNBR) compounds with dispersed polyamide droplets of 1–5 μm diameter, and little or no other filler.[28,29] Benefits cited include high strength and tear resistance, heat aging resistance, and reduced hysteresis compared to carbon black reinforced HNBR. The latter may explain recent interest in thermoplastic reinforcement for low rolling resistance tires.[30]

The present work uses the melt blending approach to reinforce amine-curable ethylene-acrylate elastomers (AEM) with a dispersion of polyamide (PA6) particles.[31] For effective elastomer reinforcement, the dispersion ideally comprises roughly spherical polyamide particles of uniform size, a diameter of ≤ 2 μm, and a volume fraction of 20–50%. In general, the melt blending approach works best to enable production of thermoplastic-reinforced vulcanizates with useful elastomeric properties when the following conditions are met:

1. The elastomer backbone and cure site (if present) have sufficient thermo-oxidative stability to withstand the melt blending process without significant degradation.
2. The thermoplastic and uncured elastomer are immiscible but highly compatible, or more preferably form covalent grafts, so the thermoplastic can disperse to a small droplet size.
3. The viscosity of the thermoplastic is greater than the elastomer, so the thermoplastic forms spherical droplets even at high volume fractions.
4. The melting point (T_m) of the thermoplastic (or glass transition temperature T_g if amorphous) is greater than both the curing and use temperatures of the article. Otherwise, the cure response of the elastomer-plastic blend suffers when curative diffuses into the fluid thermoplastic phase, and the finished article tends to deform and take a permanent set in use.

The AEM-polyamide combination meets all four requirements. AEM is typically cured and used at temperatures less than 200 °C, but can withstand short term exposure to 300 °C in an extruder. A wide variety of polyamides have melting and process temperatures within this 200 − 300 °C range. Amine curable AEM readily grafts to amine end groups of the polyamide during melt blending to promote fine dispersions. Finally, unlike many gum rubbers, AEM has relatively low viscosity (a Mooney viscosity of 20 to 30, ML 1+4 at 100 °C), whereas polyamides are available with high inherent viscosity via solid state polymerization (e.g., PA66) or directly from the reactor (e.g., PA6).

EXPERIMENTAL

Materials

The AEM elastomer is an amorphous, statistical copolymer of ethylene (70 mol %), methylacrylate (29 mol %), and a half-ester of maleic acid (1 mol %) as an amine-reactive cure site. It has a glass transition temperature of about −30 °C, an Mn of about 50,000 Daltons, and polydispersity of 3.5. The AEM is produced in DuPont facilities but is not commercially available. The PA6 is a homopolymer supplied by BASF Corporation as Ultramid®* B40 01. The PA6 has an inherent viscosity of 1.45 dl/g measured per ASTM D2857 at 25 °C using 96% by weight sulfuric acid as a solvent, and the amine end group content is determined to be 33 meq/kg by standard micro-titration method.

The N990 carbon black is Thermax®† Medium Thermal Black from Cancarb Corp., N330 carbon black is Vulcan®‡ 3 from Cabot Corp., and silica is Ultrasil® VN 3 from Evonik Industries. Primary particle size, surface area and dibutyl phthalate (DBP) oil absorption of the fillers are shown in Table I. DBP oil absorption provides a measure of the particle aggregation or structure in the filler. Greater DBP oil absorption correlates with larger aggregates of primary particles.

The amine curative for the AEM elastomer is the carbamate of hexamethylenediamine, available from The Chemours Company LLC. as Diak™§ −1. The cure accelerator is Vulcofac®¶ ACT-55, a mixture of 1,8-diazabicyclo[5.4.0]undec-7-ene (DBU) and saturated dibasic acids on an inert silica carrier (70% active) obtained from ChemSpec LTD. The process aid is Vanfre®** VAM, obtained from Vanderbilt Chemicals LLC. The antioxidant is Naugard®†† 445, obtained from Addivant USA LLC.

Equipment and Procedures

Rheological Measurements. Shear viscosities of the AEM and PA6 at 280 °C were measured using an LCR 7001 capillary rheometer (Dynisco). Mooney viscosities of the AEM and AEM-

*Ultramid® is a registered trademark of BASF Corp.
†Thermax® is a registered trademark of Cancarb Corp.
‡Vulcan® is a registered trademark of Cabot Corp. Ultrasil® is a registered trademark of Evonik Industries.
§Diak™ is a registered trademark of The Chemours Company LLC.
¶Vulcofac® is a registered trademark of Safic-Alcan.
**Vanfre® is a registered trademark of Vanderbilt Chemicals LLC.
††Naugard® is a registered trademark of Addivant USA LLC.

filler mixtures were determined according to ASTM D1646, under conditions of ML 1+10 at 121 °C, using an MV 2000 (Alpha Technologies). Cure behavior of the compounds was measured at 180 °C for 30 min, using an RPA 2000 Rubber Process Analyzer (Alpha Technologies) operating at 7% strain and 1.67 Hz. Dynamic properties of the vulcanizates were measured using the RPA 2000: the sample was first cured in the RPA 2000 at 180 °C for 30 min, and then cooled in the machine to 60 °C for strain sweeps from 0.2 to 90% strain at 0.1 Hz. Three strain sweeps were performed to eliminate transient effects, and the third sweep is reported.

Compounding. AEM – PA6 blends were produced in a twin screw extruder (Berstorff model ZE A-40 Supercompounder) operating at 300 rpm and 90 kg/hr. Energy input ranged from 680 to 780 KJ/kg, with the maximum effective shear rate in the screw estimated to be about 190 s^{-1}. PA6 was metered by weight loss feeder to the first barrel section, and the AEM was fed via a specialized rubber feeder and gear pump (The Bonnot Company). The blends exited the extruder and were underwater pelletized.

AEM was mixed with carbon black (N990, N330), and silica fillers in an internal mixer (C. W. Brabender Plasti-Corder® fitted with a Prep-Mixer® and banbury blades). The compounds were mixed for 3 min at 30rpm and 100 °C. Final mixing for all the compounds, as well as curative and additive incorporation, was conducted on a water-cooled two-roll mill (Kobelco Stewart Bolling, 8 inch).

Bound Rubber Content Determination. About 0.5 g of each rubber compound was cut into approximately 1 mm square pieces, weighed to 4 places, placed in a cage of 1000 mesh stainless steel, and the entire cage with rubber was again weighed. The cages were individually soaked in 250 mL of acetone for 3 days, removed, rinsed with fresh acetone, allowed to air dry for 1 day, and then dried 12 h in a vacuum oven at 60 °C. The cage and any remaining rubber gel were dried to determine the weight of remaining rubber gel. N990 content of the rubber gel was determined by thermogravimetric analysis (TGA Q500, TA Instruments). A 40–60 mg sample of the rubber gel was heated under nitrogen from 20 °C to 510 °C at 20 °C/min, and held for 2 min to pyrolyze the polymer. Gas was then switched to air, and ramped at 10 °C/min to burn off the carbon black. N990 carbon black itself was found to lose 0.196% weight in the initial 20 °C to 510 °C portion of the test, and the calculated polymer content of the rubber gel was compensated for this. PA6 content of the rubber gel was determined by quantifying melting endotherms using a differential scanning calorimeter (DSC Q1000, TA Instruments). A 6 to 9 mg sample of rubber gel was heated at 10 °C/min from 20 to 250 °C, cooled to 20 °C at 10/min, then reheated to 250 °C. The PA6 melting endotherm of the second heat was divided by the melting endotherm of pure PA6 after extraction in acetone like the rubber compounds (55.66 J/g). The ratio of the rubber gel melting endotherm to the pure PA6 was taken as the weight fraction of PA6 in the rubber gel. The AEM polymer itself exhibits no thermal transitions in the 160 °C to 230 °C melting range of PA6.

Assessment of Physical Properties. Specimens for tensile and hardness testing were molded into 0.2 × 7.6 × 15.2 cm plaques using a heated press (Pasadena Hydraulics model Q230C) under conditions of 180 °C for 30 min. All samples were conditioned for 24 h at room temperature and 50% RH prior to testing. Shore A hardness of the vulcanizates was determined per ASTM D2240-05 using a type-2 operating stand. The samples were 6 mm thick, composed of three 2 mm thick plies. Values reported are the median of five readings. Tensile properties were measured per ASTM D412-06, die C, using a multi-station universal tester with strain gage (tensiTECH III, Alpha Technologies). Values reported are the median of three samples tested. Compression set samples were molded under conditions of 180 °C for 10 min, followed by a post cure of 4 h at 175 °C in an air circulating oven. The samples were compressed to 75% of the original thickness in a jig, aged for one week at 150 °C in an air circulating oven, then released from the jig immediately upon removal from the oven. The specimens were allowed to cool for 30 min on a wooden board, and then measured for thickness. Compression set is calculated according to ASTM D395. Values reported are the median of three specimens.

Hot Air Aging. Specimens were hung in an air circulating oven (VWR model 1685 with rotating carousel).

Swelling and Extractable Content Determination. ASTM D395 type 1 buttons (right cylinder 12.5 mm × 29 mm) were press cured at 180 °C for 30 min, then hot air aged for 0 to 15 days at 190 °C. The buttons were sliced parallel to the large face with a mandolin slicer (Oxo) to approximately 1 mm thickness. Silicone oil was applied to the blade to improve cutting smoothness. After cutting, each slice was rinsed briefly in hexane to remove any silicone oil, and allowed to dry. The center 13 mm of each slice was stamped out, and the slice thickness measured. Each slice was then weighed, soaked in 25 mL of acetone for 3 days, then removed, blotted dry, and re-weighed. A typical slice weighed about 0.2 g before acetone exposure. The slices were then dried for 1 day at room temperature followed by 12 h at 60 °C in a vacuum oven, and reweighed. Percent swell was calculated by 100 × (swollen weight – initial weight)/(initial weight), and percent extractable was calculated by 100 × (initial weight – final dry weight)/(initial weight). The depth from the surface of a particular slice was taken to be the midpoint of the slice (i.e., the average of the distance from the nearest surface of the two faces of the slice).

RESULTS AND DISCUSSION

Polymer Viscosities and Blend Morphologies

Shear viscosities of the AEM and PA6 polymers are shown in Figure 1. The test temperature of 280 °C is within + −5 °C of the melt temperature measured during twin screw compounding of the blends. At 10 sec^{-1} shear rate the polymers have almost identical viscosities, but the AEM is more shear thinning than PA6, likely due to the relatively high polydispersity of AEM as well as branching from ethylene radical backbiting.[32,33] As a result, under typical extrusion compounding shear rates of 100 − 300 s^{-1}, the PA6 is about twice as viscous as the AEM.

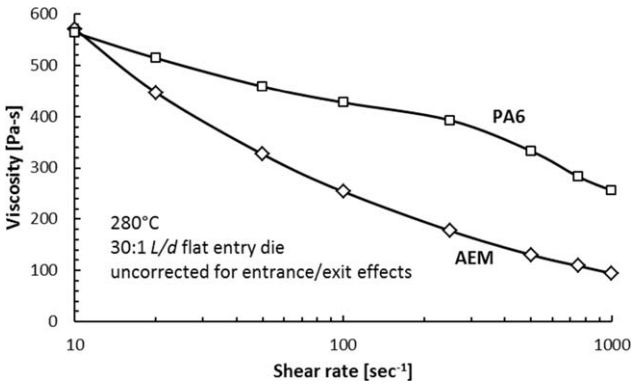

Figure 1. Shear viscosities of PA6 and AEM.

Morphologies of AEM-PA6 melt blends ranging from 30 to 60 wt % PA6 (0.292 to 0.578 volume fraction Φ) are shown in Figure 2. PA6 comprises the dispersed phase in all cases, with the largest droplets in each blend ranging from about 2 μm diameter at 30 wt % PA6, decreasing to about 1 μm diameter at 60 wt % PA6. The particle size distributions tend towards greater uniformity with increasing PA6 content. Typically, agglomeration during mixing produces the opposite trend, i.e., more frequent droplet collisions occur with increased dispersed phase volume fraction, leading to both larger droplets and a broader size distribution. The observed morphologies, therefore, suggest that agglomeration in this system is highly depressed. Further support for this view may be derived from the ordering that develops with increasing PA6 content, particularly evident in Figure 2(d). To maximize packing, the PA6 droplet shapes in some regions deviate from spherical to accommodate the nearest neighbors. Such a phenomenon can occur only in the presence of a highly effective "soap"—ostensibly grafted AEM molecules on the surface of the PA6 droplets. As a result of the low agglomeration rates, PA6 droplet size becomes dominated by the applied shear stress. As content of the high viscosity PA6 in the blend increases, the increasing shear stress therefore produces smaller PA6 droplets. Some of the PA6 particles in Figure 2 contain small inclusions, particularly at higher PA6 levels, which are probably entrapped AEM. The fraction of encapsulated AEM in each blend has not been quantified.

Mixtures of AEM and N990 Carbon Black

The AEM-PA6 blend morphologies in Figure 2 indicate that the PA6 is a large particle, low surface area, zero structure filler, and as such might be expected to provide relatively poor reinforcement of thermoset rubber. A conventional filler of comparable size and structure is medium thermal carbon black (MT black or N990), having primary particles ranging from about 0.2 to 0.5 μm diameter, a surface area of 8–10 m^2/g, and minimal structure (particle aggregates). Photomicrographs of AEM-N990 blends at filler volume fractions equivalent to the AEM-PA6 blends above are shown in Figure 3. The N990 particles appear as misshapen spheres, about 2 to 5 times smaller than the PA6 droplets in Figure 2, with increasing particle aggregation as carbon black level rises. The aggregates are irregular in shape, ranging from one to several microns in size.

Bound Rubber

Bound rubber is the fraction of rubber in an uncured rubber-filler mixture that cannot be extracted by a good solvent for the rubber. Although bound rubber measurements strongly depend on the mixing history of the blend and the extraction conditions, certain trends are recognized. For example, bound rubber content tends to correlate positively with increasing carbon black surface activity, structure, and decreasing particle size.[2,5,13,34–36] Bound rubber can strongly affect the reinforcing properties of a filler. For example, it is well known that graphitizing carbon black decreases surface activity and leads to large losses in vulcanizate modulus, tensile strength, and abrasion resistance.[13,34] When an elastomer-filler blend is extracted with solvent, high levels of bound rubber lead to formation of a swollen elastomer-filler gel. Gel formation becomes more prevalent with increasing filler loading, and the filler loading at the onset of gel formation decreases with decreasing filler particle size.[34,37]

The fraction of gel-bound rubber in the AEM blends of Figures 2 and 3 are shown in Table II. An unfilled AEM control contains zero gel by this test method. The N990 mixtures contain almost no bound rubber gel up to 0.477Φ, and even at the highest N990 level of 0.578Φ, over 90% of the blend extracted into the solvent. The small amount of gel remaining in this sample was made up almost entirely of N990 (2 wt % AEM in the gel), and of the total AEM polymer in the blend, only 0.6% by weight remained bound in the gel. These low levels of bound rubber are in line with expectations based on the large particle size, low structure, and low surface activity of N990 carbon black.[34]

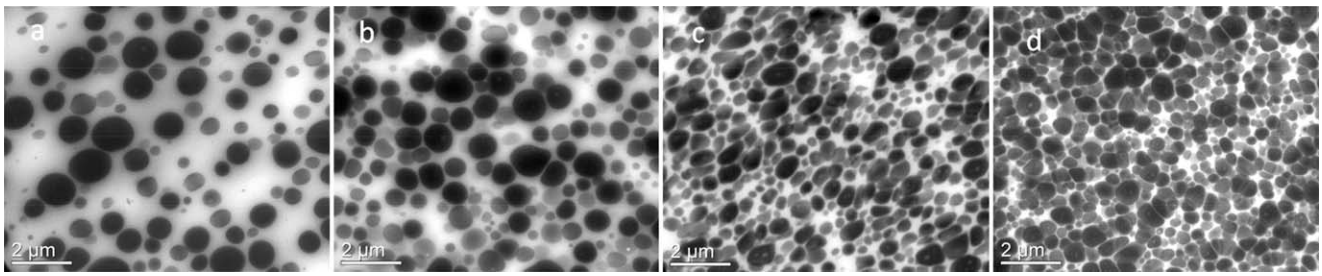

Figure 2. Transmission electron micrographs of AEM-PA6 blends with differing PA6 content. Blend produced via twin screw extrusion. The PA6 phase is stained dark. PA6 weight percent and volume fraction (Φ) are given below. (a) 30 wt % (0.292Φ) (b) 40 wt % (0.378Φ) (c) 50 wt % (0.477Φ) (d) 60 wt % (0.578Φ).

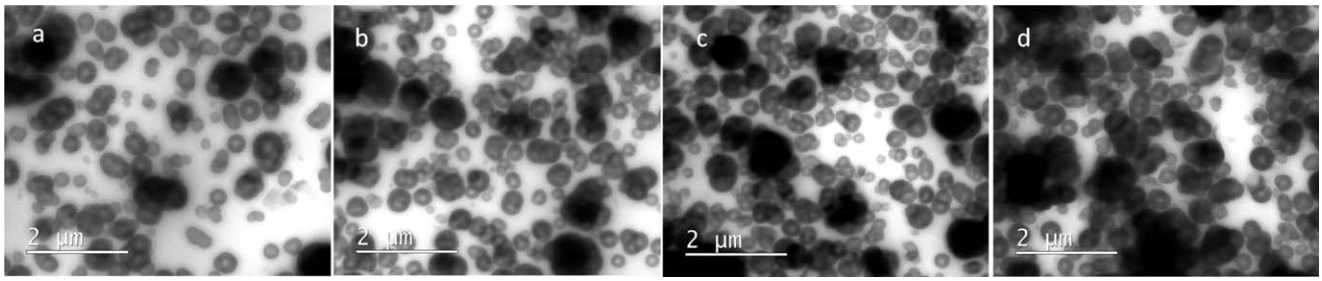

Figure 3. Transmission electron micrographs of AEM-N990 mixtures with differing carbon black content, compounded in an internal mixer followed by roll milling. N990 weight percent and volume fraction (Φ) are given below. (a) 42.6 wt % (0.292Φ) b) 52.3 wt % (0.378Φ) c) 62.2 wt % (0.477Φ) d) 71.2 wt % (0.578Φ) N990 carbon black appears as the dark phase.

The PA6 blends generally display much higher levels of gel-bound rubber than the N990 mixtures. At a PA6 level of 0.292Φ the sample extracts almost completely into the solvent leaving no gel, but the rubber-filler gel level rises rapidly with increasing PA6 (Figure 4). At the highest PA6 level (0.578Φ), close to half of the initial AEM content of the blend remains in the gel, providing strong evidence of AEM-PA6 grafting. Figure 4 shows that between PA6 volume fractions of 0.378 − 0.578, the percent of the total AEM content of the blend that remains unextracted in the gel rises linearly with PA6 content. This linear relationship suggests that the specific surface area of the PA6 and the thickness of the grafted shell of AEM rubber remain essentially constant over this range of PA6.

Blend Rheology

Figure 5 shows relative viscosities (μ_r) of AEM-N990 mixtures and AEM-PA6 blends as a function of filler volume fraction, compared with the Einstein model and the Guth-Gold extension.[38,39] The N990 and PA6 compositions closely match each other over most of the range, with the N990 mixtures deviating to higher viscosity only at the highest filler volume fraction (0.578Φ). This deviation correlates with the onset of measurable bound rubber-N990 gel. N990 aggregates may be the root cause of both the bound rubber gel and the viscosity deviation from the PA6 blends. Indeed, the bound rubber-N990 gel at this high filler level consists almost entirely of carbon black aggregate, with very little AEM polymer.

The Einstein viscosity model for dilute, non-interacting suspensions of spheres fits well for both the AEM-N990 and AEM-PA6 compositions up to about 0.3Φ, beyond which it underestimates viscosity. Brennan *et al.* have suggested that the adsorbed layer of bound rubber be treated as part of the filler, thereby increasing the effective filler volume fraction.[40] Indeed, the AEM-PA6 blends deviate from the Einstein model at a PA6 volume fraction where measurable rubber-filler gel appears. Applying this correction based on the bound rubber data in Table II, however, still leaves Einstein model strongly underestimating blend viscosity at PA6 volume fractions greater than 0.3. The Guth-Gold extension of the Einstein model, designed to account for filler-filler interactions, overestimates viscosity over most of the range, except at the highest N990 level. These results suggest that blends studied here, ranging from 0.292Φ to 0.578Φ, comprise a mixture of interacting and non-interacting particles. Fewer isolated, non-interacting particles remain as the filler volume fraction increases, though the mechanism for interactions apparently differs between N990 and PA6. N990 particles tend to form aggregates with filler-filler contact, whereas the PA6 particles are tethered by grafted AEM molecules.

Curing the AEM-PA6 Blends and AEM-N990 Mixtures

AEM-N990 and AEM-PA6 compositions are converted into curable compounds by roll mill mixing curative, cure accelerator, process aid, and anti-oxidant at 1, 2, 0.5, and 2 phr, respectively. The molar ratio of amine curative to AEM cure site in the recipe is 0.9. Cure responses at 180 °C of the N990 and PA6 filled compounds, as well as an unfilled control sample, are shown in Figure 6(a). The compounds with PA6 particles cure more slowly, but to a higher final torque. Figure 6(b) examines these differences explicitly, plotting the maximum torque and the

Table II. Bound Rubber Measurements of AEM-N990 Carbon Black Mixtures and AEM-PA6 Blends

Filler volume fraction (Φ)	0	0.292	0.378	0.477	0.578	0.292	0.378	0.477	0.578
Filler type	None	N990	N990	N990	N990	PA6	PA6	PA6	PA6
Weight % of sample remaining as gel after extraction	0	0.5	0.4	1.3	9.1	0.2	39.0	57.5	69.4
Appearance of extract in acetone	Clear	Black	Black	Black	Black	White	Hazy	Clear	Clear
Weight % AEM in the gel	0	nm	nm	nm	2.0[a]	nm	1.2[b]	24.3[b]	26.6[b]
Weight % of total AEM prior to extraction remaining in the gel	0	nm	nm	nm	0.6	nm	7.3	27.9	46.2

nm, not measured.
[a] Determined by ash content (TGA).
[b] Determined by integrating PA6 melting endotherm (DSC).

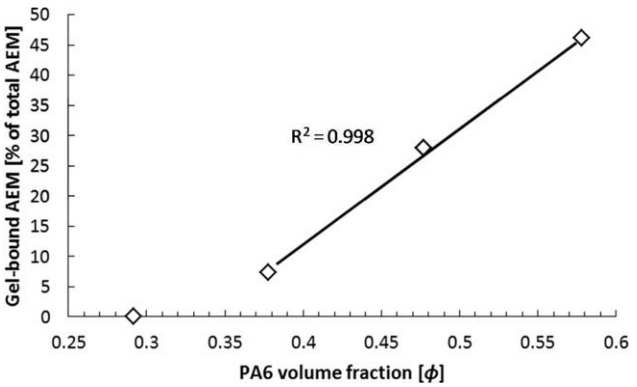

Figure 4. Percent of AEM rubber remaining bound in AEM-PA6 gel after extraction with acetone, as a function of PA6 volume fraction (data from Table II).

time to 90% cure (t90) as a function of Φ. Cure rate of the PA6-based compounds decreases linearly with Φ, such that at the highest PA6 content, t90 is about three times greater than the unfilled control. The N990 compounds, however, show a slight trend in the opposite direction, towards increasing cure rate. These results may be explained by two factors: the bound rubber content of the PA6 compounds, and the slight basicity of N990 carbon black. Bound rubber cannot be intimately mixed with curative, and these molecules crosslink only as curative diffuses from the non-bound regions of AEM polymer. Therefore as bound rubber content rises with linearly with PA6 content, so does t90. The consumption of AEM cure site to produce bound rubber probably contributes only slightly to the cure rate decrease. For example, a 60 wt % PA6 blend dispersed in 1 μm diameter droplets, assuming full reaction of all the PA6 amine chain ends within a 50 nm surface layer of the droplet, would consume less than 7% of the available AEM cure site. For the N990 blends the basicity of N990 contributes slight cure acceleration, since the amine curing reaction is base catalyzed.

Bound rubber in the PA6 blends also leads to higher maximum torque than the N990 compounds. In effect, the PA6 particles act as macroscopic, multi-functional crosslink sites. While the maximum torque is a function of both uncured compound viscosity and crosslinks formed during the curing process, the N990 and PA6 blends have almost identical uncured viscosities over the range 0.292 to 0.477Φ. Thus the steadily widening maximum torque difference between the PA6 and N990 compounds over this range must result from the additional crosslinks generated by bound rubber fraction of the PA6 blends. At 0.578Φ, N990 aggregation boosts the uncured compound viscosity, and therefore maximum torque δ between N990 and PA6 blends narrows at this highest filler level.

The Hardness and Tensile Properties of N990 and PA6 Reinforced Vulcanizates

In rubber technology, the term "reinforcement" is loosely applied, but generally refers to an increase in properties such as tensile modulus (particularly at strains > 100%), tensile and tear strengths, and hardness. Of these, Shore A hardness is probably most fundamental, since many rubber applications have well defined hardness requirements. As shown in Figure 7, N990- and PA6-filled vulcanizates have nearly identical Shore A hardnesses for a given filler volume fraction, paralleling the viscosity results of Figure 5. By this measure, the PA6 particles are relatively nonreinforcing, in line with expectations for a large particle, unstructured filler.

Tensile properties, however, follow a different trend. Figure 8 illustrates the engineering stress-strain properties of the various vulcanizates, showing that PA6 reinforces AEM far more effectively than N990 carbon black. Over a filler volume fraction of 0.292 to 0.578 the tensile strength of the PA6 filled vulcanizates increases from 17.6 to 34.6MPa, while that of the N990 vulcanizates decreases from 12.4 to 8.6MPa. The phenomenon of decreasing tensile strength with increasing N990 level is accompanied by a yielding behavior at volume fractions of 0.378 and greater, which suggests de-bonding of the rubber from the N990 filler. The drop in tensile strength at the higher N990 levels may result from agglomerates that easily break apart under stress, creating flaws and premature fracture (note agglomerates in Figure 3). In contrast, the PA6 compounds exhibit high modulus at elongations of 100% and greater and no yielding even at the highest PA6 level, at the expense of lower elongation to break than the unfilled or N990 vulcanizates. These results are consistent with AEM-PA6 grafting, resulting in both an increase in the effective crosslink density compared to the N990 filled compounds [see Figure 6(a)], as well as suppression of AEM-PA6 de-bonding under stress.

The Dynamic Properties of N990 and PA6 Reinforced Vulcanizates

An enormous variety of fillers is used in rubber compounds, primarily because any given filler brings both advantages and disadvantages. Perhaps the most widely studied phenomenon where filler characteristics largely control the response of a rubber vulcanizate involves the nonlinear decrease in storage modulus with increasing strain, known as the Payne effect.[7] While the source of the Payne effect is still an active research area,

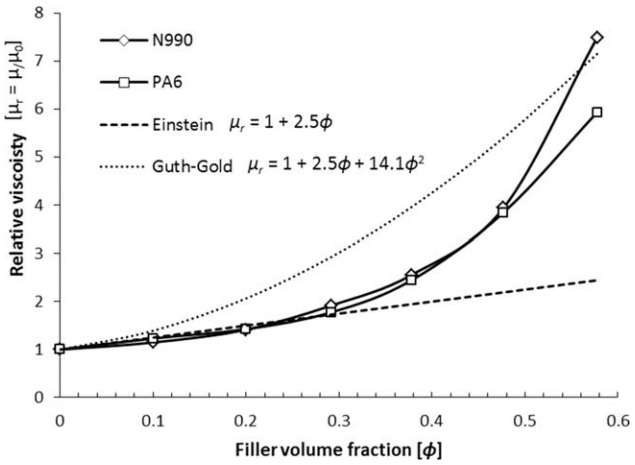

Figure 5. Relative viscosity of AEM-filer blends, as a function of filler volume fraction. $\mu_0 = 18.2$ for the N990 blends [unfilled Mooney viscosity (ML 1 + 10, 121 °C)] and 16.0 for the PA6 blends, the difference attributable to shear degradation in the twin screw extruder. Data points at 0.1Φ and 0.2Φ obtained by diluting the 0.292Φ blends with the appropriate amount of AEM by roll mill mixing.

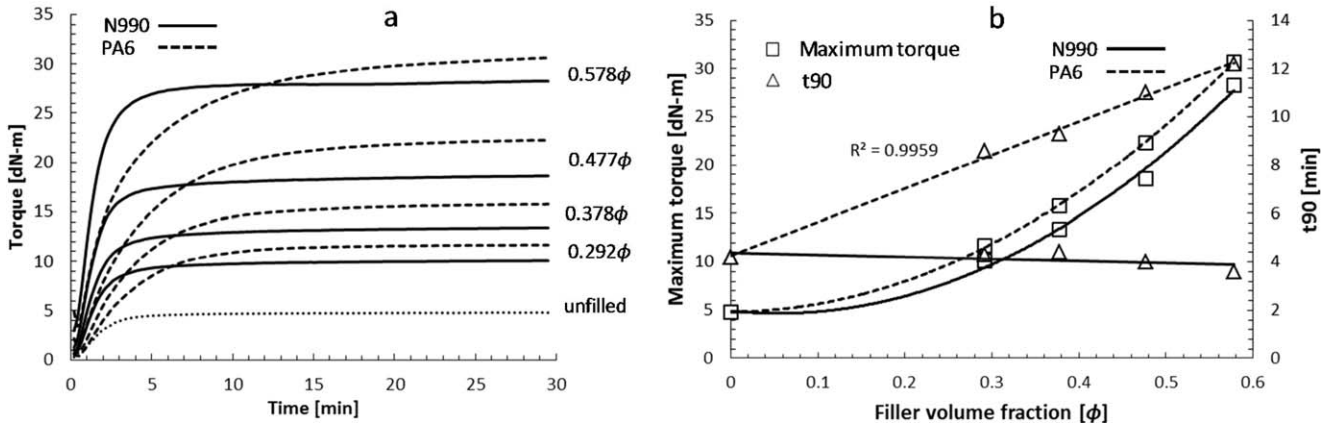

Figure 6. (a) Cure response of compounds as measured by torque as a function of time at 180 °C, biconical oscillating die rheometer, 7% strain, 1.67 Hz. (b) Statistics derived from the cure responses: maximum torque and t90 (time to 90% of the difference between the maximum and minimum torques) as a function of filler volume fraction.

there is general agreement that strain-induced breakdown of the filler network is the primary cause, augmented by disentanglement of elastomer chains from the filler surface.[6,13,15] Structured fillers with high surface area (i.e., small primary particles) offer excellent physical properties such as tensile strength, tear strength and abrasion resistance, but also increase the tendency for filler networking as well as labile polymer-filler interactions, thereby increasing the strain softening tendency of the vulcanizate. Thermoplastic particles may avoid this tradeoff by providing strength enhancement, without inducing a large Payne effect due to the absence of a filler network and reduced slippage of polymer chains at the filler surface as a result of AEM-PA6 grafting.

The compositions shown in Table III permit comparisons of the Payne effect in AEM vulcanizates with a variety of fillers. In addition to the N990 carbon black and PA6 discussed so far, compounds are produced with two highly reinforcing fillers composed of nano-scale primary particles: N330 (HAF) carbon black and precipitated silica. Note that the compositions in Table III contain differing filler levels, both in terms of weight (phr) and volume fraction. The filler levels here are selected, as is typical industrial practice, to achieve a given vulcanizate hardness, in this case 55-60 Shore A. Because primary particle size decreases in the order PA6 > N990 > N330 > silica while surface area and structure simultaneously increase, a decreasing volume fraction of filler is needed to achieve a given hardness across this series. Note that Mooney viscosity of the blends increases in the same order, ranging from 31 for the PA6 blend to 72 for the silica blend, in spite of decreasing filler volume fraction. The viscosity trend likely results from increasing filler networking across this series (discussed below), which increases the effective volume of the filler and thus viscosity of the blend.

The AEM-filler compositions of Table III, as well as an unfilled control, are converted into curable compounds as described previously and cured for 30 min at 180 °C. The storage moduli and tan δ (G''/G') as a function of shear strain of the vulcanizates are shown in Figure 9. The unfilled AEM exhibits almost no strain softening, while the Payne effect of the filled vulcanizates increases in the order PA6 = N990 < N330 ≪ silica. The large Payne effect of the N330 and silica compounds is consistent with the high reinforcing ability of these fillers due to their nano-scale primary particle size, as well as high surface area and structure (see Table I). PA6, however, provides the unusual combination of high reinforcement with low Payne effect. The similarity in the strain softening of PA6 and N990, in spite of the dramatic difference in terms of filler-polymer bonding, suggests that the Payne effect is not reduced simply by preventing disentanglement of polymer chains from the filler surface. Indeed, it is reasonable to assume that bonding polymer chains to a filler surface simply shifts the disentanglement process to the next layer of unbonded polymer chains, which then disentangle and re-entangle with the relatively immobile polymer molecules fixed to the filler surface. In this scenario, attaching polymer molecules to the filler surface only affects where the disentanglement occurs, without appreciably altering the magnitude of the phenomenon. Historically, it has been difficult to separate filler-filler and polymer-filler components of the Payne effect by studying rubber with conventional inorganic fillers,

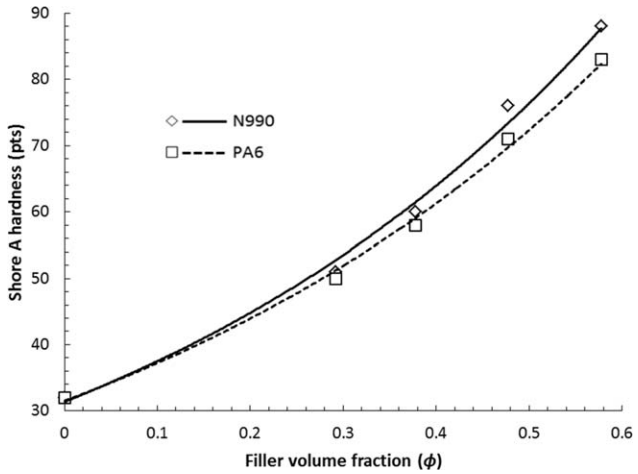

Figure 7. Shore A hardness of N990 and PA6 filled vulcanizates as a function of filler volume fraction.

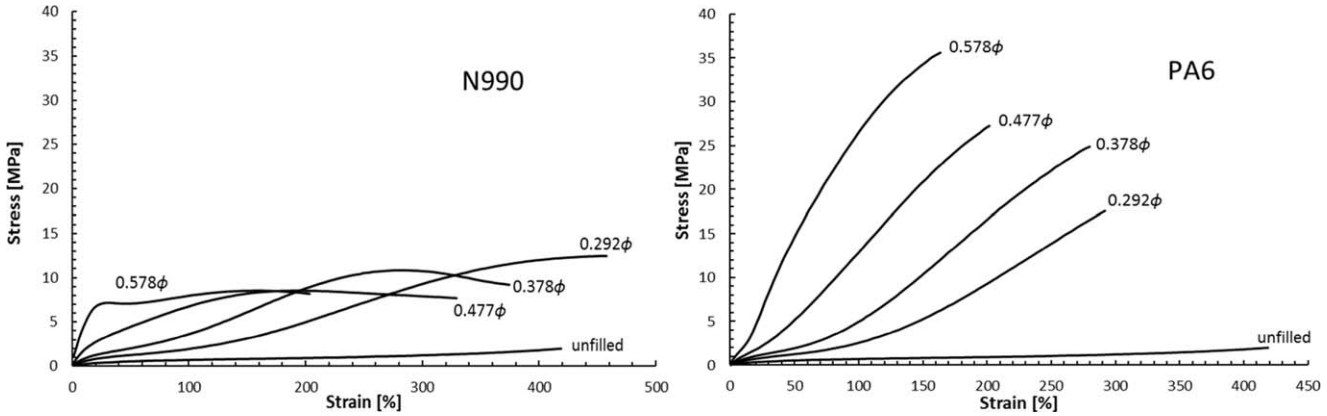

Figure 8. Stress−strain curves for N990 (left) and PA6 (right) filled compounds having filler volume fraction of 0 to 0.578.

carbon black, or even unusual fillers like crosslinked polymer emulsions or glass spheres. The difficulty stems from the fact that in a liquid-solid blend, filler–filler and polymer–filler interactions cannot be varied independently: increasing the affinity of the solid for the liquid (i.e., rubber) phase simultaneously decreases the affinity of the solid for its neighbors, thus unavoidably reducing filler-filler interactions. In the case of liquid-liquid blends (e.g., melt blending thermoplastic with rubber), direct filler-filler contact becomes impossible. Collisions of molten thermoplastic droplets simply produce a single droplet of larger size by coalescence, not aggregates of small droplets. Melt mixed rubber-thermoplastic blends therefore provide a unique opportunity to study the origins of the Payne effect.

While the Payne effect is essentially independent of rubber crosslink level, the same is not true for tan δ (G''/G'). The number of effective network chains per unit volume of rubber (ν) can be estimated by measuring the swell of each vulcanizate in a good solvent, and applying the Flory-Rehner equation modified to account for the presence of fillers by the method of Kraus.[41,42] Using group molar attraction constants of Hoy, and assuming 100% reaction of the curative, the solubility parameter of the AEM vulcanizate is estimated to be 18.15 $MPa^{1/2}$.[43] Using acetone as the solvent, the Flory-Huggins interaction parameter (χ) for acetone-AEM vulcanizate at 20 °C can be estimated by the method of Bristow and Watson.[44] Assuming a lattice constant of 0.34, and acetone molar volume and solubility parameter of 74 cm^3 and 19.8 $MPa^{1/2}$ respectively, χ is estimated to be 0.423.

Using the above approach, Figure 10 shows the estimates of the number effective network chains (ν, units of mols × 10^4 cm^{-3}) in each of the vulcanizates from Figure 9. Working with sulfur cured SBR filled with carbon black or silica, Kraus observed that fillers can either increase or decrease ν. Increasing ν results from polymer-filler linkages, which are generally small in number, and the more dominant effect of filler-filler attachments (i.e., formation of a filler network), which acts like a secondary network in the vulcanizate.[42] On the other hand, fillers can decrease ν if they interfere with the function of the curative or accelerator (the latter noted by Kraus in the case of silica—SBR compounds).

The results in Figure 10 illustrate both these phenomena. Compared to the unfilled vulcanizate, the N990 and N330 containing vulcanizates have almost 50% greater ν, whereas the PA6 vulcanizate ν is nearly double that of the unfilled. Given that the N990 and N330 levels have been chosen to achieve similar vulcanizate hardnesses, the equivalence in their contribution to ν seems reasonable. The higher structure of N330 compared to N990, which should strongly contribute to both ν and vulcanizate hardness, is moderated by the lower volume fraction of N330 versus N990 in the compound (0.181 versus 0.307). The large ν for the PA6 vulcanizate confirms the high graft levels of the PA6 and AEM polymers inferred previously based on gel content (Table II), cure response (Figure 6), and tensile properties (Figure 8). Interestingly, because the PA6 vulcanizate completely lacks filler-filler contacts, the PA6 contribution to ν must result entirely from physical AEM-PA6 attachments. Put another way, almost half of the elastically active AEM network chains are at some point attached to a PA6 droplet. The silica containing vulcanizate provides an example of cure inhibition at the filler surface, leading to reduced ν compared to the unfilled compound. The acidic surface of the silica probably protonates the basic accelerator and/or amine curative, retarding the cure. The silica compound indeed gave a very slow cure with a t90 of 17.7 min, compared to 6.4 min for the unfilled control.

Table III. AEM–filler blends, Mooney Viscosities and Filler Volume Fractions

AEM–filler blends	phr	phr	phr	phr
AEM polymer	100	100	100	100
N990 carbon black	80			
N330 carbon black		40		
Silica (precipitated)			45	
PA6				49.3
Mooney viscosity, ML 1 + 10, 121 °C	36	38	72	31
Filler volume fraction (Φ)	0.307	0.181	0.149	0.310

The carbon black and silica fillers are blended into the AEM using a small internal mixer, followed by roll milling, while the PA6 blend is prepared by twin screw extrusion.

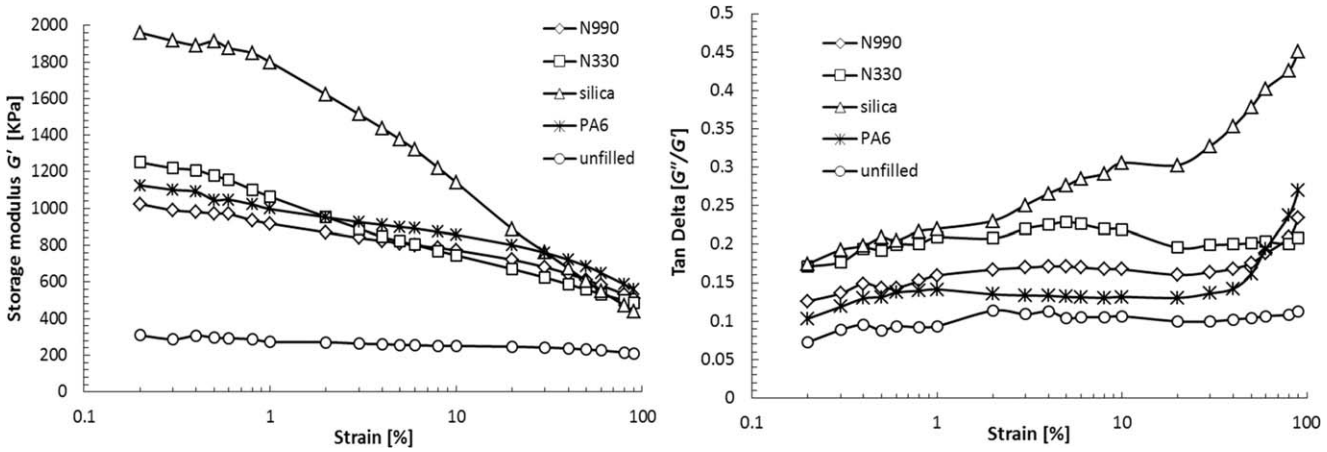

Figure 9. Storage modulus and tan δ (G''/G') as a function of shear strain for AEM vulcanizates cured at 180 °C for 30 min. Unfilled control compound is included. Test conditions of 60 °C, 0.1 Hz.

Turning back to the tan δ (G''/G') data in Figure 9, the strain dependence of tan δ for crosslinked, filled elastomers depends strongly on the test temperature. At the 60 °C, well above the T_g of AEM, the main source of energy dissipation during cyclic strain is thought to be related to changes in the filler network structure.[13] Consistent with this notion, the unfilled vulcanizate in Figure 9 exhibits the lowest tan δ (least energy dissipation), with almost no strain dependence. When a filler network is present, tan δ increases at all strains relative to an unfilled compound, and furthermore a maximum generally appears around 10% strain. The N330 vulcanizate and to a lesser extent the N990 vulcanizate both exemplify this behavior, indicating the presence of a filler network, or at least some filler−filler contact. The silica vulcanizate exhibits somewhat of an anomaly, in which a local tan δ maximum occurs around 10% strain, but beyond 20% strain tan δ rises rapidly. The viscous loss at high strains may result from the cure inhibition at the silica surface, in which the poorly cured rubber is pulled away from the silica surface at high strains. Due to the combined effect of a low state of cure and a strong filler network, the silica vulcanizate has the highest tan δ across the strain spectrum. Perhaps the most interesting tan δ response, however, comes from the PA6 vulcanizate. The PA6 tan δ is nearly as low as the unfilled compound, with little strain dependence out to about 30% strain, beyond which it rises strongly, exceeding the tan δ of both the N990 and N330 vulcanizates. The simplest explanation for the high strain response of the PA6 vulcanizate may be that it has the highest filler volume fraction ($\Phi = 0.310$), and therefore the highest strain amplification of the rubber phase, combined with the least rubber to recover the strain. In other words, at some critical macroscopic strain, the rubber phase undergoes segmental motions of sufficient magnitude that the network can no longer respond elastically within the time scale of the test. This explanation, if correct, should apply with nearly the same force for the N990 vulcanizate ($\Phi = 0.307$). In fact, the N990 vulcanizate does exhibit a tan δ rise at high strain, though to a lesser extent than the PA6 vulcanizate. I propose that the high strain tan δ response of the PA6 vulcanizate results from the low rubber content, further magnified by PA6-AEM grafting. As discussed previously, a large fraction of the elastically active network includes an attachment to at least one PA6 particle, and these PA6 particles effectively "anchor" a portion of the rubber network. Small strains can be accommodated by AEM molecules far from a PA6 particle, but when the strain is large enough to displace the PA6 particles and create large scale segmental motions in the AEM network, the same PA6-AEM attachments that afford high strength encumber the elastic recovery. For the N990 vulcanizate, AEM molecules are relatively free to desorb from the surface of an N990 particle, enabling the network to recover more quickly from large strains, though at the expense of tensile strength and modulus (Figure 8).

Filler Effects in Diffusion Limited Oxidation

The influence of filler reinforcement on the dynamic properties of rubber has been widely studied, mostly in the tire industry. On the other hand, elastomers find use in applications where dynamic properties have little or no impact on product performance, such as static seals, gaskets, hoses, conveyor belts, and cable jacketing. Particularly for under-hood automotive applications, the ability of a rubber article to resist elevated temperature creep and oxidation are of prime importance. Since thermoplastics are relatively soft, ductile, and oxidizable compared to carbon black or inorganic fillers, they may seem a

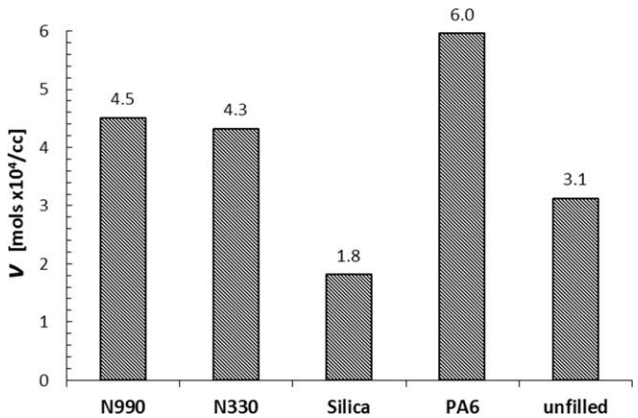

Figure 10. Estimates of the number of elastically effective network chains per unit volume of AEM rubber (ν), for the AEM vulcanizates of Figure 9.

poor choice for elastomer reinforcement in these applications. Surprisingly, the reverse is true, at least for AEM-PA6.

Compression set resistance has traditionally been used in the rubber industry to measure elastomer creep, and in turn estimate the useful life of static seals. The test involves compressing a standardized specimen, typically by 25%, and holding it in the compressed state for a certain time and temperature. The specimen is then released from the fixture immediately upon removal from the oven (or freezer), allowed to recover for a set period, and measured to determine the percent permanent deformation or "set". Although other tests more directly correlate with seal life, compression set testing is simple, widely used, and sensitive to factors that affect elastic recovery. In particular, compression set tends to increase (become worse) as the filler in the rubber compound becomes more reinforcing, even when compared in vulcanizates of constant hardness. The rearrangement of a filler network under heat and stress is generally considered to produce this response.

Figure 11 plots compression set after one week at 150 °C in a hot air oven, using the AEM vulcanizates containing PA6, N990, N330 and silica fillers described previously. Test specimens of varying surface area/volume ratio (*S/V*) are used for each compound: a large ASTM D395 type 1 button, a smaller ISO 815 type B button, and an ASTM D214 o-ring. The compression set results correlate inversely with the density of elastically active network chains (see Figure 10), and in the case of the N990 and N330 vulcanizates where this crosslink density is about equal, in manner consistent with the degree of filler networking. Beyond these straightforward results, creep of the dispersed PA6 droplets apparently contributes little towards permanent deformation, since the AEM-PA6 vulcanizate achieves the lowest compression set in the group. Significantly, compression set of all the vulcanizates increases with the *S/V* of the test specimen. The N990 and N330 vulcanizates in particular show the greatest specimen shape sensitivity.

The response of AEM compression set to *S/V* is consistent with heterogeneous, diffusion limited oxidation of the vulcanizates during the compression set test, a phenomenon documented by Dole and Chauchard for N774 carbon black filled AEM aged at 150 °C in air.[45–49] Oxidative degradation of AEM produces a combination of scission and crosslinking, both of which limit the ability of the network to recover from deformation. Because compression set sensitivity to *S/V* varies with the filler type, the data in Figure 11 suggest that fillers might play a role in heterogeneous oxidation, a proposition that has received little attention to date.

Most rubber technologists recognize that filler type and level can affect elastomer hot air aging performance. Recommendations to limit carbon black content in compounds designed for optimal hot air aging may be found in literature of some rubber suppliers, notably EPDM and ACM types. Mostafa *et al.* found that unfilled SBR and NBR vulcanizates exhibit better oxidative resistance than those containing N550 carbon black.[50] Edge *et al.* studied oxidation of peroxide and sulfur cured NR vulcanizates, finding that compounds containing small particle, high structure carbon blacks oxidize more quickly than compounds

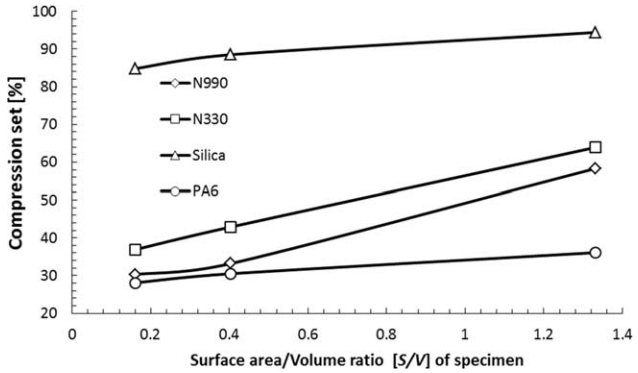

Figure 11. Compression set measured after one week at 150 °C for the AEM-filler blends of Table III, converted to curable compounds and cured at 180 °C/10 min, then post cured at 175 °C for 4 h. ASTM and ISO buttons are right cylinders of $d \times H$ of 29 × 12.5 mm and 13 × 6.3 mm, respectively. The D214 o-ring has an outer diameter of 24.99 mm cross-sectional diameter of 3.53 mm.

filled with large particle carbon black.[51] They suggest that the results may stem from an antagonistic effect between the amine anti-oxidant and carbon black. Wise *et al.* provide the only known comparison of elastomer oxidation profiles with and without carbon black.[52,53] They find that 56.5 phr of N774 carbon black in NBR decreases the activation energy for oxygen uptake and increases the rate of surface modulus growth during hot air aging, compared to an otherwise identical unfilled vulcanizate. Wise *et al.* use a phenolic anti-oxidant. The acceleration of elastomer degradation due to fillers is not limited to carbon black. Gabrielle *et al.* use solid state NMR to conclude that EPDM undergoes scission near the surface of ATH particles during hot air aging, forming an ever-expanding layer of degraded polymer around each filler particle.[54] On the other hand, studies of elastomer oxidation do not always find fillers to be antagonistic. Delor-Jestin *et al.* report that carbon black (unspecified type) reduces the formation rate of carbonylated species during heat aging of EPDM.[55] They attribute the beneficial effect to phenolic moieties on the carbon black surface.

The present work examines in two ways the relationship of filler type to hot air aging performance of AEM vulcanizates. The first method is typical of industrial and automotive applications, where tensile specimens are stamped out of molded plaques and hung in a circulating air oven for aging. The necked-in portion of the tensile specimen has a relatively large *S/V* (3.0 for a typical 2 mm thick plaque), so surface oxidation strongly influences the results. Figure 12 shows elongation at break (E_b) and stress at 10% strain (M10) as a function of hot air aging time at 190 °C, using AEM vulcanizates with fillers as shown in Table III as well as an unfilled AEM compound.

The hot air aging response of the AEM vulcanizates falls into two distinct groups. Unfilled and PA6 filled vulcanizates show a relatively stable or moderately declining E_b and M10 for the entire aging period, whereas the N990, N330, and silica reinforced vulcanizates experience fast declines in E_b and rising M10. After 15 days at 190 °C, the N990, N330, and silica filled vulcanizates are an order of magnitude stiffer than the PA6

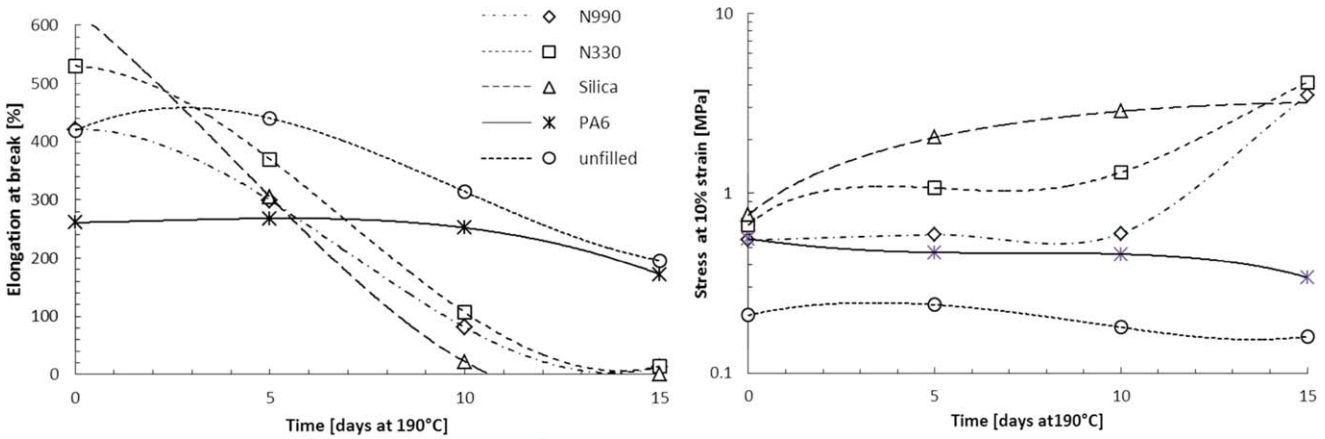

Figure 12. Tensile elongation at break and stress at 10% strain of AEM vulcanizates as a function of hot air aging time at 190 °C. ASTM D412 die C specimens, about 2 mm thick. [Color figure can be viewed in the online issue, which is available at wileyonlinelibrary.com.]

reinforced vulcanizate. How can fillers alter AEM hot air aging so dramatically? Perhaps a clue may be found in the dynamic properties of the vulcanizates. Note that the rate of change in Eb and M10 follows the same ranking as the degree of filler networking determined by the Payne effect and tan δ measurements (silica > N330 > N990).

The second approach to examining filler effects during hot air aging of AEM replaces the high *S/V* tensile specimen with 29 x 12.5mm right cylinders having an $S/V = 0.16$ (ASTM type 1 compression set button). Each cylinder is sliced into ~1 mm think layers (parallel to the flat face) for analysis after heat aging. Figure 13 shows a composite image of slices from PA6 and silica reinforced vulcanizates after 10 days at 190 °C, taken near the axial center of the button. The darkened oxidation zone appears to have penetrated about four times more deeply into the silica compound than the PA6 reinforced compound. In reality, the visual assessment considerably underestimates the damage to the silica compound, as described below.

To evaluate the oxidation profiles of the specimens, a 13 mm diameter punch is taken from the middle of each ~1 mm thick slice, thereby minimizing oxygen diffusion from the sides of the cylinder. The center punches are swollen to equilibrium in acetone, weighed, then dried and reweighed. The weight gain of each punch approximates the net effect of crosslinking and scission caused by oxidation, averaged over the depth range of the slice. Because oxidation likely alters the solubility parameter of the AEM, no attempt is made to translate solvent swell into crosslink density. The extractable content of each slice provides an indication of the dominant oxidation process (crosslinking or scission) at a given time and location in the sample. By considering both swell and extractables, important trends in the oxidation profiles as a function of filler type become apparent.

The trends in solvent swell and extractable content as a function of average distance from the nearest polymer-air surface are shown in Figure 14. To begin, note that all the unaged samples are quite uniform—the percent weight gain and extractable content are essentially independent of depth from the nearest face. The differences in acetone swell between the unaged compounds correlate with the crosslink density measurements of Figure 10, while the unaged extractable content remains within a surprisingly narrow band of about 6–8%, even though the AEM polymer content of the samples ranges from 94.8 wt % (unfilled) to 53.9 wt % (N990).

Before dissecting the oxidation profiles of the individual vulcanizates, it is helpful to propose the general responses of AEM polymer to oxygen and heat that fit the data of Figure 14. Under high oxygen conditions like the surface layer, AEM initially undergoes mainly chain scission, probably due to

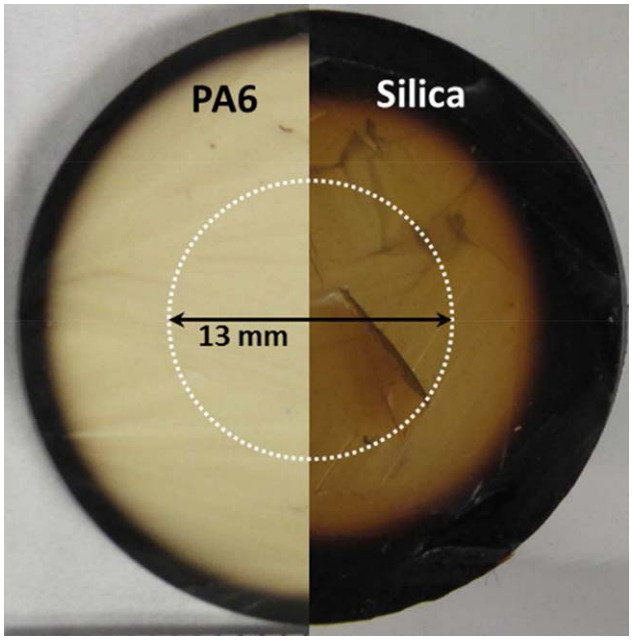

Figure 13. Composite view of ~1 mm thick slices taken from heat aged cylinders (ASTM type 1 compression set buttons). The slices are taken near the axial midpoint (about 6mm from the flat face) after aging for 10 days at 190 °C in a hot air oven. The PA6 reinforced AEM vulcanizate is shown on the left, the silica reinforced on the right. The dotted line illustrates the 13 mm disk punched from the center of each slice, used to measure acetone swell and extractable content. [Color figure can be viewed in the online issue, which is available at wileyonlinelibrary.com.]

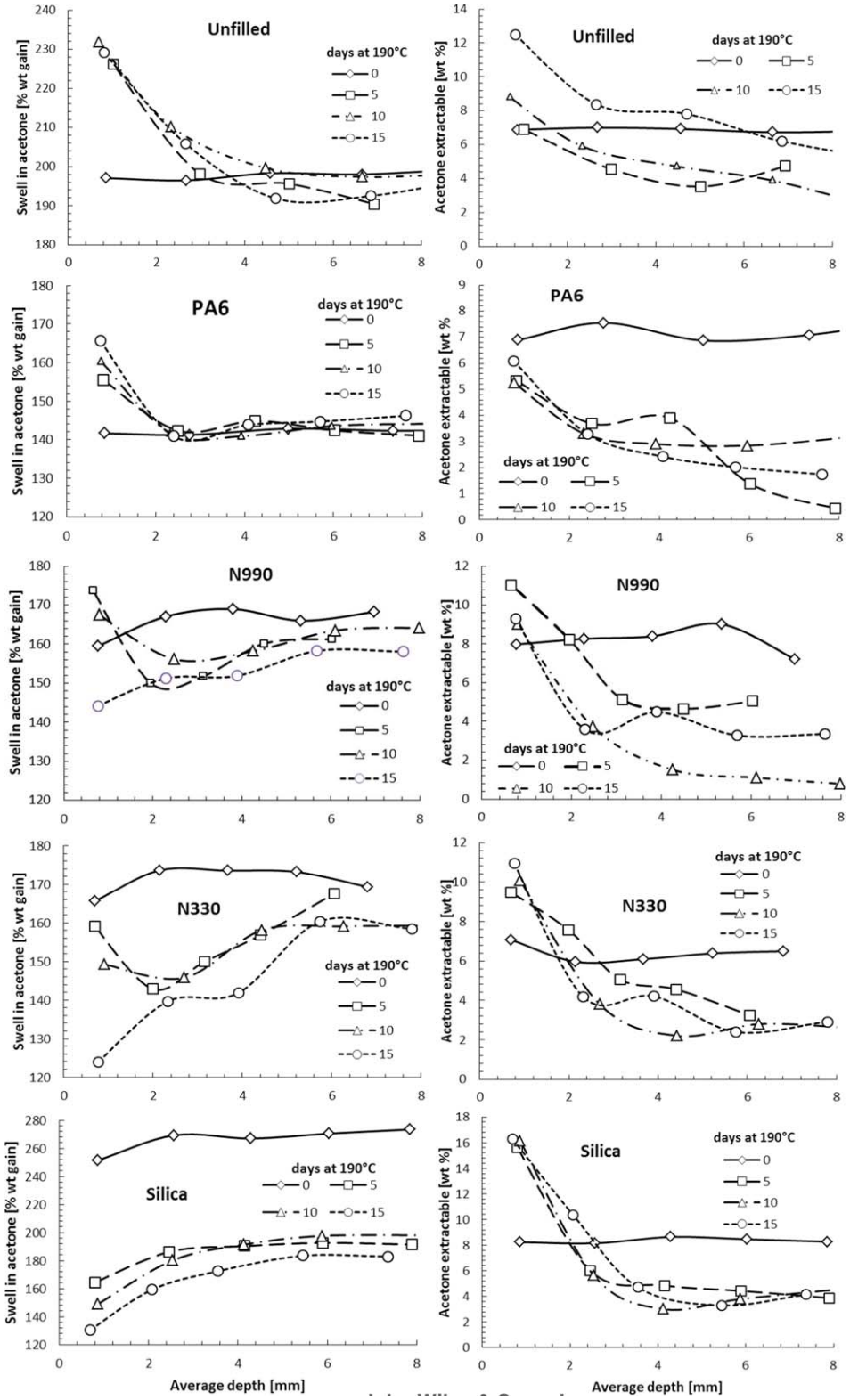

Figure 14. Equilibrium weight gain in acetone and weight loss upon drying of ~1 mm thick slices from AEM vulcanizates molded into ASTM compression set buttons (right cylinders $d = 29$ mm, $h = 12.5$ mm), and aged for 0 to 15 days at 190 °C in a hot air oven. Buttons sliced parallel to one of the faces, and the center 6.3 mm disk cut out for the swell and extractable measurement. Average depth is the distance from the axial center of the slice to the nearest flat face of the button. Percentages based on the total sample weight (not corrected for filler content). [Color figure can be viewed in the online issue, which is available at wileyonlinelibrary.com.]

oxidation at the tertiary carbons formed due to backbiting of the ethylene radical during polymerization.[33] As oxidation proceeds, scission continues to generate extractable polymer fragments, but crosslinking reactions also set in. The crosslinking slows and eventually reverses the increasing solvent swell caused by scission. These crosslinking reactions partly involve transesterification, although radical processes may also play a role.[48] Under continued aging, crosslinking initiated in the outer layer propagates through to the center of the sample, the rate of which dramatically influences the durability of the vulcanizate under heat aging conditions.

The unfilled and PA6 reinforced vulcanizates exhibit similar heat aging profiles: net chain scission in the surface layer throughout the aging, and little or no crosslinking in the core. This behavior is consistent with the good retention of tensile elongation and a slightly decreasing tensile modulus during heat aging of the 2 mm thick tensile specimens for these compounds (Figure 12). The unfilled sample appears to permit greater permeation of oxygen, because surface layer scission extends to about 3 mm in depth, compared to less than 2 mm deep for the PA6 reinforced sample. In addition, the center of the unfilled sample shows evidence of oxidation due to mild crosslinking and scission, whereas the PA6 sample exhibits no change in swell and only a decrease in extractables. The generally lower oxidation compared to the unfilled AEM may result from oxygen scavenging by the PA6 via the well-known process of radical attack at the N-vicinal methylene group.

The AEM samples with conventional fillers exhibit more complex oxidation profiles, and all three exhibit a wave of highly crosslinked material propagating from surface to core. The rate of propagation correlates with the magnitude of the Payne effect for these compounds, which in turn correlates with increasing structure and surface area of the fillers (Table I). The N990 filled sample may be considered transitional, combining features of both the unfilled and PA6 filled AEM compounds with those of the N330 and silica containing AEM compounds. Like the unfilled and PA6 filled samples, the surface of the N990 filled compound initially exhibits increased swell and extractables, pointing to net scission. After 5 days of aging, however, the trend reverses and both swell and extractables begin to decrease. Ultimately, the surface layer has a lower solvent swell (apparently more crosslinked) than in the unaged state, a feature not found in the unfilled or PA6 filled compounds. Surface crosslinking at the 15 day aging period is corroborated by the increased M10 of the 2 mm thick N990 samples at this aging interval, shown in Figure 12. The interior of the N990 sample has lower extractable content and only minor decrease in solvent swell, suggesting low oxygen levels throughout the aging. The very center has the lowest oxygen content, indicated by the smallest decrease in swell combined with almost zero extractables. These results explain why, of the AEM compounds containing conventional fillers, the N990 compound exhibits the best heat aging durability.

The aging profile of the N330 reinforced vulcanizate is qualitatively similar to the N990 vulcanizate, though accelerated. After 5 days at 190 °C, the surface layer has already passed through the net scission phase into net crosslinking, and it continues to decrease strongly in swell over the remainder of the aging. After 15 days, solvent swell exhibits a steep gradient from surface to core as the crosslinking propagates inwards. The N330 sample has the same trend in extractables as the N990 sample (greatest at the surface, decreasing towards the core), but at all points the extractables for the N330 compound are greater than the N990, suggesting higher oxygen levels throughout the sample. These results are in agreement with those of Figure 12, where the N330 exhibits quicker changes in tensile elongation and modulus compared to the N990 compound.

The silica reinforced compound further accelerates the trends shown in the N990 and N330 compounds. After just 5 days at 190 °C, solvent swell has decreased dramatically, and presents an almost uniform level from surface to core. The surface extractables are greater than any other sample, and the core extactables are greater than for all but the unfilled sample. The silica reinforced vulcanizate apparently oxidizes quickly from surface to core during heat aging, a conclusion corroborated by the rapid change in elongation at break and modulus as shown in Figure 12.

It is worth noting that the dependence of compression set on *S/V* is in agreement with the present analysis of oxidation profiles for the four filled compounds. The PA6 filled compound has only a slight increase in compression set with increasing *S/V*, because oxidation extends only a short distance into the compression set specimen. The silica compound also shows only a small influence of *S/V* on its already poor compression set, because oxidative degradation penetrates so quickly through the sample. The N990 and N330 vulcanizates, however, have a stronger dependence of compression set on *S/V* because the oxidation profile moves at an intermediate pace. Specimens with high *S/V* become more uniformly oxidized and have worse (greater) compression set than those with low *S/V*.

How do conventional particulate fillers like carbon black and silica increase the rate of diffusion limited oxidation in elastomers? The present results suggest a physical rather than a chemical mechanism, driven primarily by incomplete elastomer-filler wetting and decreased bulk oxygen permeability, amplified by increasing filler surface area and filler–filler contacts. For example, Le *et al.* show that NBR rubber mixed with silica reaches an equilibrium wetting of about 65% of the silica surface area, while NR wets only about half as much.[56] Because less than perfect wetting of conventional particulate fillers seems to be the rule rather than the exception, a filler particle located at the surface not only displaces elastomer, it generates some elastomer-air interface. The combination effectively increases the *S/V* of the surface elastomer layer. As filler particle size decreases, the thickness of the affected surface layer may decrease, but the decreased inter-particle spacing and greater filler surface area (of which some fraction is not wetted) rapidly drive up *S/V*. Filler-filler contacts, which become more likely as particle size decreases, could thicken the affected surface layer by permitting some communication between elastomer-filler gaps located at the surface with those embedded slightly deeper (note that filler-filler contact inherently precludes complete

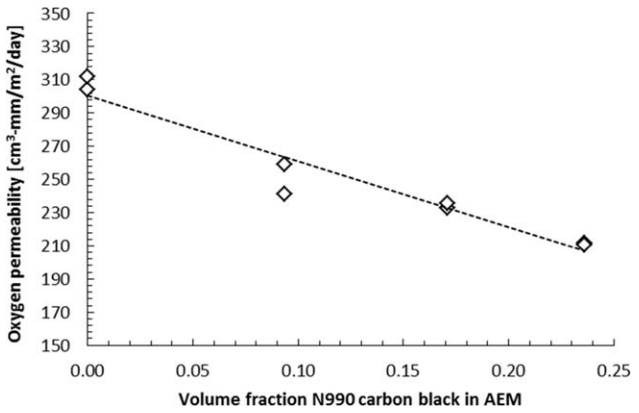

Figure 15. Oxygen permeability at 23 °C, 50% RH of ~0.8 to 1.5 mm thick films of AEM containing 0% to 24% by volume N990 carbon black. Measured per ASTM D3985.

wetting of the filler surface by polymer). At the same time, carbon black and inorganic fillers themselves are largely impermeable to oxygen, and therefore present a tortuous path for oxygen diffusion through the bulk. Figure 15 shows the decrease in oxygen permeability of AEM filled with up to 24% by volume N990 carbon black. The net result is that conventional fillers increase not only the surface layer *S/V* of a rubber article, but also surface layer oxygen level as the filler slows diffusion into the bulk. These two factors cause a thin oxidized surface layer to rapidly form, and in the case of AEM, to transition from net scission of mild oxidation to net crosslinking characteristic of severe oxidation. Note that the high surface oxygen content of a filled compound initially results in lower bulk oxygen content than an unfilled compound – this is why the bulk extractable contents of the N990 and N330 compounds are low compared to the unfilled AEM. While the filler initially protects the bulk polymer in early stages of heat aging, crosslinking of the surface AEM apparently causes shrinkage, opening gaps between the AEM and filler. These gaps in turn expose fresh AEM directly below the surface to high oxygen levels, and the process repeats. Eventually, net crosslinking penetrates the entire sample, leading to catastrophic embrittlement. The unfilled AEM avoids this fate by spreading the oxidation more uniformly throughout the thickness, thereby remaining in the net scission phase throughout the 15 day/190 °C aging period.

In view of the above mechanism, it becomes clear why AEM reinforced with a PA6 dispersion exhibits superior resistance to hot air aging. Mixing AEM with PA6 in a molten state ensures complete wetting of the polymer-filler interface, so the *S/V* of the vulcanizate surface layer is not increased versus the unfilled state. PA6 is permeable to oxygen, especially at temperatures above T_g, allowing oxygen to diffuse away from the surface, which in turn reduces the tendency for degradation to focus on the surface layer as with the conventional fillers.[57] The PA6 droplets also reduce or eliminate the aggravating factors found in conventional reinforcing fillers, i.e., high surface area and filler-filler contacts. Finally, PA6 droplets themselves oxidize, which has the effect of narrowing the surface oxidation zone and reducing bulk oxygen levels compared to an unfilled AEM.

CONCLUSIONS

Melt mixing amine-curable AEM rubber and PA6 can produce dispersions of approximately 0.5 to 2 μm sized PA6 droplets in a continuous phase of AEM, up to a PA6 volume fraction (Φ) of nearly 0.6. The blends remain processable by conventional rubber compounding techniques at temperatures below the melting point of the PA6, and may be compounded and cured to form vulcanizates with attractive properties.

PA6 droplets differ in several important aspects from carbon black or silica fillers commonly used in rubber compounds. Reaction between the AEM cure sites and PA6 amine end groups yields extensive grafting during melt blending. At PA6 $\Phi = 0.578$, nearly half the AEM remains as bound rubber during solvent extraction of the uncured blend, whereas the same volume fraction of N990 carbon black produces almost no bound rubber. In spite of the difference in bound rubber, PA6 droplets and N990 carbon black yield blends of similar viscosity for a given filler volume fraction, both exhibiting a positive deviation from the Einstein viscosity model at $\Phi > 0.3$. In other areas, however, bound rubber from AEM-PA6 grafting does affect compound and vulcanizate properties. Bound rubber moderately slows the cure rate, significantly increases the number of elastically active network chains per unit volume in the vulcanizate, and yields vulcanizates with high tensile strength, up to three times stronger than an otherwise equivalent N990 filled vulcanizate.

Dispersed PA6 droplets also differ from conventional particulate fillers in that the PA6 droplets are completely wetted by AEM; consequently, the AEM-PA6 vulcanizates have no filler-filler contacts. PA6 reinforced vulcanizates exhibit a small but nonzero Payne effect, almost identical to that of an AEM vulcanizate reinforced with N990 carbon black. This observation indicates that bonding polymer chains to a filler surface does not decrease the Payne effect per se, but simply shifts the strain softening associated with polymer chain desorption from a filler surface to a functionally similar disentanglement process between filler-bonded and unbonded chains.

Finally, the grafted and fully wetted PA6 droplets differ from conventional fillers in that they are permeable to oxygen and relatively oxidizable. In combination, these attributes dramatically extend the lifetime of AEM vulcanizates during hot air aging under conditions of diffusion limited oxidation. Solvent swell and extraction tests on sections of AEM vulcanizates exposed to 190 °C air reveal distinct differences in degradation profiles between unfilled or PA6-reinforced vulcanizates, and vulcanizates reinforced with carbon black (N990, N330), or precipitated silica. While the surface layer of the unfilled and PA6 reinforced vulcanizates undergoes net scission throughout the 15 days of aging, the surface of vulcanizates containing conventional fillers progresses through the scission phase into net crosslinking due to extensive oxidation. An oxidized crosslinked "wave front" then advances through the thickness of the sample, leading to embrittlement and catastrophic loss of properties. The rate of progression of the crosslinked wave front correlates with the magnitude of the Payne effect in the vulcanizate, suggesting that filler-filler contacts play a role. AEM vulcanizates

containing highly structured fillers with nano-scale primary particles (N330 carbon black, precipitated silica) exhibit a large Payne effect and rapid progression of this oxidized wave front.

ACKNOWLEDGMENTS

The author wishes to express appreciation to J. Mikolajczyk for the compounding, molding, and generating most of the data contained this report, and also to S. Dunlap for the TEM images. The author gratefully acknowledges support and permission to publish from DuPont. This report is dedicated to my father, Dr. R. A. Oriani, who inspired my scientific curiosity.

REFERENCES

1. Kraus, G. *Agnew. Makromol. Chem* **1977**, *60/61*, 215.
2. Kraus, G.; Gent, A. N. In Science and Technology of Rubber; Eirich, F., Ed.; Academic Press: New York; 2nd ed.; Chapter 8, p 339 and Chapter 10, p 419, **1978**.
3. Boonstra, B. B. In Rubber Technology and Manufacture; Blow, C. M.; Hepburn, C., Eds.; Butterworth Scientific: London **1982**; 2nd ed.; Chapter 7, p 269.
4. LeBlanc, J. L. In Filled Polymers: Science and Industrial Applications; CRC Press: Boca Raton, FL; Chapter 5, p 91 and Chapter 6, p 236, **2010**.
5. Donnet, J. B.; Voet, A. In Carbon Black; Marcel Dekker: New York; Chapters 7-9, p 214, **1976**.
6. Bokobza, L. *Macromol. Mater. Eng.* **2004**, *289*, 607.
7. Payne, A. R. *J. Appl. Polym. Sci.* **1962**, *6*, 57.
8. Boonstra, B. B.; Medalia, A. I. *Rubber Chem. Technol.* **1963**, *36*, 115.
9. Berriot, J.; Montes, H.; Martin, F.; Mauger, M.; Pyckhout-Hintzen, W.; Meier, G.; Frielinghaus, H. *Polymer* **2003**, *44*, 6131.
10. Le, H. H.; Ilisch, S.; Radusch, H. J. *Polymer* **2009**, *50*, 2294.
11. Medalia, A. I. *Rubber Chem. Technol.* **1972**, *45*, 1171.
12. Edwards, D. C. *J. Mater. Sci.* **1990**, *25*, 4175.
13. Wang, M. *J. Rubber Chem. Technol.* **1998**, *71*, 520.
14. Dannenberg, E. M. *Rubber Chem. Technol.* **1986**, *59*, 512.
15. Termonia, Y. *Polymer* **2001**, *51*, 4448.
16. Liu, Y.; Li, L.; Wang, Q. *J. Appl. Polym. Sci.* **2010**, *118*, 1111.
17. Harison, S.; Brown, W. U.S. Patent 2,538,779 (**1951**).
18. Morton, M.; Murphy, R. J. *Polym. Prepr., Am. Chem. Soc., Div. Polym. Chem.* **1973**, *14*, 481.
19. Morton,M. In Multicomponent Polymer Systems, Advances in Chemistry Series; Platzer, N., Ed.; American Chemical Society: Washington DC, Chapter 31, p 490, **1971**.
20. Cai, J. J.; Salovey, R. *J. Mater. Sci.* **1999**, *34*, 4719.
21. Hoffman, W. In Rubber Technology Handbook, Hanser: New York, Chapter 3, p 71; **1989**.
22. Ebnesajjad, S.; Morgan, R. A. In Fluoropolymer Additives; Morgan, S. E. A., Ed.; William Andrew Publishing: Oxford, **2012**; Chapter 10, p 175.
23. Stewart, C. W. *J. Appl. Polym. Sci.* **1993**, *48*, 809.
24. Logothetis, A.; Stewart, C. U.S. Patent 4,713,418, **1987**.
25. Yamamoto, S.; Fujii, K.; Kurihara, H.; Wada, T. U.S. Pat. 5,948,503, **1999**.
26. Ma, J.; Feng, Y. X.; Xu, J.; Xiong, M. L.; Zhu, Y. J.; Zhang, L. Q. *Polymer* **2002**, *43*, 937.
27. Park, E. H.; Walker, F. J. U.S. Patent 7,608,216, **2009**.
28. Betremieux, I.; Alex, P.; Marcq, P.; Dousson, C. U.S. Patent 6,133,375, **2000**.
29. Liu, X.; Huang, H.; Zhang, Y.; Zhang, Y. *Polym. Polym. Comp.* **2003**, *11*, 179.
30. Gandon-Pain, S.; Hut, A. U.S. Patent 8,883,929, **2014**.
31. Oriani, S. R. U.S. Patent 8,779,044, **2014**.
32. Wu, Y. T.; Stewart, M. A.; Ye, Y. U.S. Patent 7,608,675, **2009**.
33. McCord, E. F.; Shaw, W. A.; Hutchinson, R. A. *Macromolecules* **1997**, *30*, 246.
34. Kraus, G. *Rubber Chem. Technol.* **1965**, *38*, 1070.
35. Roychoudhury, A.; De, P. P. *J. Appl. Polym. Sci.* **1995**, *55*, 9.
36. Pliskin, I.; Tokita, N. *J. Appl. Polym. Sci.* **1972**, *16*, 473.
37. Karasek, L.; Sumita, M. *J. Mater. Sci.* **1996**, *31*, 281.
38. Einstein, A. *Annalen Der Physik* **1906**, *19*, 289.
39. Guth, E.; Gold, O. *Phys. Rev.* **1938**, *53*, 322.
40. Brennan, J. J.; Jermyn, T. E.; Boonstra, B. B. *J. Appl. Polym. Sci.* **1964**, *8*, 2687.
41. Flory, P. J.; Rehner, J. Jr. *J. Chem. Phys.* **1943**, *11*, 521.
42. Kraus, G. *Rubber Chem. Technol.* **1957**, *30*, 928.
43. Hoy, K. L. *J. Paint Tech.* **1970**, *42*, 76.
44. Bristow, G. W.; Watson, W. F. *Trans. Faraday Soc.* **1958**, *54*, 1731.
45. Dole, P.; Chauchard, J. *Macromol. Chem. Phys.* **1994**, *195*, 3949.
46. Dole, P.; Chauchard, J. *Polym. Degrad. Stabil.* **1995**, *47*, 441.
47. Dole, P.; Chauchard, J. *Polym. Degrad. Stabil.* **1995**, *47*, 449.
48. Dole, P.; Chauchard, J. *Polym. Degrad. Stabil.* **1996**, *53*, 53.
49. Dole, P.; Chauchard, J. *J. Appl. Polym. Sci.* **1997**, *65*, 2507.
50. Mostafa, A.; Abouel-Kasem, A.; Bayoumi, M.; El-Sebaie, M. *J. Mater. Des.* **2009**, *30*, 791.
51. Edge, M.; Allen, N.; Gonzalez-Sanchez, R.; Liauw, C.; Read, S.; Whitehouse, R. *Polym. Degrad. Stabil.* **1999**, *64*, 197.
52. Wise, J.; Gillen, K.; Clough, R. *Polym. Degrad. Stabil.* **1995**, *49*, 403.
53. Celina, M.; Wise, J.; Ottesen, D.; Gillen, K.; Clough, R. *Polym. Degrad. Stabil.* **1998**, *60*, 493.
54. Gabrielle, B.; Lorthioir, C.; Laupretre, F. *J. Phys. Chem. B* **2011**, *115*, 12392.
55. Delor-Jestin, F.; Lacoste, J.; Barrois-Oudin, N.; Cardinet, C.; Lemaire, J. *Polym. Degrad. Stabil.* **2000**, *67*, 469.
56. Le, H. H.; Hamann, E.; Ilisch, S.; Heinrich, G.; Radusch, H. J. *Polymer* **2014**, *55*, 1560.
57. Ito, M.; Nagai, K. *J. Appl. Polym. Sci.* **2010**, *118*, 928.